



Article submitted to journal

**Subject Areas:**

xxxxx, xxxxx, xxxx

**Keywords:**

Taylor–Couette flow, transition to turbulence, dynamical systems, pattern formation

**Author for correspondence:**

Marc Avila

e-mail:

marc.avila@zarm.uni-bremen.de

Routes to turbulence in  
Taylor–Couette flowDaniel Feldmann<sup>1</sup>,Daniel Borrero-Echeverry<sup>2</sup>,Michael J. Burin<sup>3</sup>, Kerstin Avila<sup>4,5</sup> andMarc Avila<sup>1</sup><sup>1</sup>Universität Bremen, Center of Applied Space Technology and Microgravity (ZARM), 28359 Bremen, Germany.<sup>2</sup>Department of Physics, Willamette University, Salem, OR 97214, USA.<sup>3</sup>Department of Physics, California State University - San Marcos, San Marcos, CA 92096, USA.<sup>4</sup>Universität Bremen, Faculty of Production Engineering, 28359 Bremen, Germany.<sup>5</sup>Leibniz Institute for Materials Engineering (IWT), 28359 Bremen, Germany.

Fluid flows between rotating concentric cylinders exhibit two distinct routes to turbulence. In flows dominated by inner-cylinder rotation, a sequence of linear instabilities leads to temporally chaotic dynamics as the rotation speed is increased. The resulting flow patterns occupy the whole system and lose spatial symmetry and coherence in this gradual transition process. In flows dominated by outer-cylinder rotation, the transition is abrupt and leads directly to turbulent flow regions which compete with laminar ones. We here review the main features of these two routes to turbulence and illustrate them with direct numerical simulations. Bifurcation theory rationalises the origin of temporal chaos in both cases. However, the catastrophic transition of flows dominated by outer-cylinder rotation can only be understood by accounting for the spatial proliferation of turbulent regions with a statistical approach. We stress the role of the ratio of Coriolis to shear forces and demonstrate that the lower border for the existence of intermittent laminar-turbulent patterns is determined by the rotation number.

## 1. Background

Fluid flows tend to become turbulent as their speed increases. The emergence of turbulence is characterised by erratic fluctuations of fluid velocity and pressure, which enhance dissipation and thus lead to increased energy losses. In his seminal 1923 paper, Taylor [1] computed the instability of laminar flows between co-rotating cylinders mathematically rigorously by starting from the Navier–Stokes equations. His own experimental verification of this result established hydrodynamic stability theory as a powerful tool to make accurate predictions of flow instability. To understand how remarkable this accomplishment is, it is necessary to review the historical background [2]. Interest in the problem of transition was spurred by Osborne Reynolds’ 1883 paper on turbulence transition in pipe flow [3]. Reynolds showed experimentally that in pipes this transition is sudden and depends on the level of disturbances present in the experiment. He concluded that *“the condition might be one of instability for disturbance of a certain magnitude and stable for smaller disturbances.”* Despite his remark, most of the subsequent theoretical approaches to the problem of transition, such as those pioneered by Orr [4], Sommerfeld [5] and others, focused on the evolution of infinitesimal disturbances and thus failed to predict transition in pipe flow and even in the mathematically more tractable case of plane shear flow [2].

This failure of linear hydrodynamic stability theory to explain Reynolds’ experiments, and the insurmountable difficulties inherent to nonlinear theories, continued to trouble the scientific community for forty years. Then Taylor made the key observation that *“the study of the fluid stability when the disturbances are not considered as infinitely small is extremely difficult. It seems more promising therefore to examine the stability of liquid contained between concentric rotating cylinders. If instability is found for infinitesimal disturbances in this case it will be possible to examine the matter experimentally”* [1]. Taylor’s proposal was motivated by Mallock’s experiments in which the inner cylinder was rotated while the outer cylinder was held fixed [6]. Mallock observed that the flow became unstable even at the lowest speeds that he considered. These observations would go on to inspire Lord Rayleigh’s derivation of a criterion for the stability of rotating inviscid fluids [7]. Taylor extended this analysis to include viscous effects by applying Orr’s framework to the Navier–Stokes equations in cylindrical coordinates, keeping curvature terms up to first order. His calculations of the onset of instability were for the first time in excellent agreement with laboratory experiments. He showed this for different curvatures, as determined by the radius ratio  $\eta = r_i/r_o$ , where  $r_i$  and  $r_o$  are the radii of the inner and outer cylinders, respectively. Furthermore, the corresponding axially periodic eigenfunctions, which take on the form of toroidal vortices stacked along the axial direction, were in good agreement with his flow visualisation experiments using dye injections. Taylor’s analysis was able to predict the stability of the flow even in regimes where Rayleigh’s theory [7] had failed, such as when the cylinders are made to counter-rotate or in experiments where the inner cylinder is made to rotate with very low velocity. More generally, Taylor’s paper was also instrumental in confirming the validity of the Navier–Stokes equations, supplemented with no-slip boundary conditions, beyond the laminar regime.

An intriguing result of Taylor’s 1923 analysis, supported by his experiments, was that laminar flows with a stationary inner cylinder are linearly stable. This conflicted with earlier observations by Couette [8], who observed that the torque exerted on the inner cylinder scaled linearly at low angular speeds of the outer cylinder,  $\Omega_o$ , but became erratic as  $\Omega_o$  was increased above a certain critical threshold, before stabilising but exhibiting a stronger (nonlinear) scaling at even higher  $\Omega_o$ . Couette’s results agreed with observations by Mallock [6], who also noted that if the system was run right below the threshold for transition and a small perturbation was introduced, the torque measurements became erratic for extended periods of time before the system returned to its initial quiescent state. This transient nature of turbulence is a landmark of linearly stable flows (see, e.g., Avila *et al.* [9] for a recent review) and will be discussed later in § 4(b).

Similar experiments were carried out by Wendt [10] at even higher Reynolds numbers. Wendt also studied the effects of the end-wall conditions in his apparatus (e.g., attaching the cap at the bottom of his test section to the inner/outer cylinder) and showed that these could change

the critical rotation rate for transition by as much as 10%. Although Taylor initially attributed the increased torque reported by Couette, Mallock, and Wendt to end-wall effects caused by the short aspect ratio  $\Gamma = h/d \lesssim 20$  of their experimental apparatus (here,  $h$  is the cylinders' height and  $d = r_o - r_i$  is the size of the gap between them), he was later able to reproduce their observations with a new, longer and more accurate apparatus [11]. Furthermore, Taylor showed that the transition could be triggered by purposely applying slight perturbations and that turbulence remained sustained well below the threshold for natural (uncontrolled) transition. This bi-stability of laminar flow and turbulence at fixed Reynolds numbers, reported earlier by Reynolds for pipe flow [3], is another landmark of linearly stable flows (see, e.g., [12]). Taylor also studied the effect of varying the system geometry and extrapolated his data toward the narrow gap limit,  $\eta \rightarrow 1$ , to infer that the critical Reynolds number for plane Couette flow should lie between 315 and 500, which is in agreement with more recent experiments [13–15]. In the 1950s, Schultz-Grunow impressively showed that if the apparatus was fabricated with stringent tolerances, circular Couette flow could be maintained up to Reynolds numbers exceeding 40 000, whereas if he purposely misaligned his apparatus or used cylinders that were not perfectly round, his system would transition at Reynolds numbers consistent with earlier studies [6,8,10,11].

The early work by Taylor and others made it clear that flows between concentric cylinders exhibit two distinct routes to turbulence. The differences between these routes were pinpointed in a decade-long study published by Coles [16]. In the first route, characteristic of flows dominated by inner-cylinder rotation, transition occurs via a sequence of instabilities that increase the temporal complexity of the flow and decrease its spatial symmetry. Coles characterised this sequence using hot wire anemometry and flow visualisations. For the second route, characteristic of flows dominated by outer-cylinder rotation, Coles noted that transition to turbulence is akin to that reported by Reynolds for pipe flow [3]. It is controlled by the evolution of finite-amplitude perturbations, which lead to the sudden emergence of localised turbulent domains interspersed in a laminar background. In this paper, we review previous works on the transition to turbulence in Taylor–Couette flow and analyse them from the perspective of nonlinear dynamical systems. The main concepts are illustrated with results from new direct numerical simulations (DNS).

## 2. Parameter regimes of Taylor–Couette flow

Traditionally, the different dynamical regimes of Taylor–Couette flow have been characterised in terms of two Reynolds numbers: the outer Reynolds number ( $Re_o = r_o \Omega_o d / \nu$ ) and the inner Reynolds number ( $Re_i = r_i \Omega_i d / \nu$ ). They are based on the size of the gap between the cylinders ( $d$ ), the tangential velocity of each cylinder ( $u_o = r_o \Omega_o$  and  $u_i = r_i \Omega_i$ , respectively), and the kinematic viscosity of the fluid ( $\nu$ ). An example of a stability diagram using these traditional set of parameters is shown in Fig. 1(a) for a system with  $\eta = 0.5$ . The laminar circular Couette flow (hereafter termed C) is linearly (centrifugally) unstable above the neutral stability curve shown in red. For a given value of  $Re_o$ , there is a critical  $Re_i$  above which the flow becomes unstable and secondary flows with increasing complexity emerge. The neutral stability curve shown here is analogous to those computed by Taylor [1], but we discretise the full Navier–Stokes equations linearised about C with a Galerkin method [17]. The transition to turbulence in this region (red in Fig. 1) is discussed in § 3.

Below the neutral stability curve, the flow is linearly stable and only finite-amplitude disturbances can trigger turbulence. Linearly stable Taylor–Couette flows are classified into two distinct regimes with qualitatively different physics. In the cyclonic regime (shaded in green in Fig. 1), the vorticity of the flow and the mean angular velocity are aligned. Here, the flow may exhibit a subcritical transition to turbulence. This transition scenario is reviewed in § 4. By contrast, in the anti-cyclonic (quasi-Keplerian) regime, which is characterised by radially increasing angular momentum, but radially decreasing angular velocity, the weight of evidence suggests that no transition to turbulence occurs even at Reynolds numbers exceeding a million. The quasi-Keplerian regime (blue in Fig. 1) is discussed in § 5.

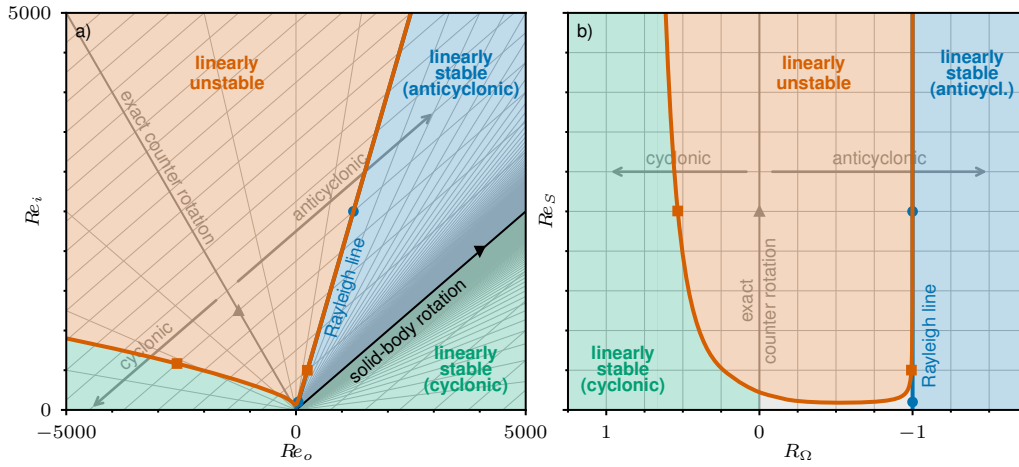


**Figure 1.** (a) Parameter space of Taylor–Couette flow spanned by the inner and outer cylinder Reynolds numbers,  $Re_i$  and  $Re_o$ , respectively, for  $\eta = 0.5$ . In the region above the neutral stability curve (shown in red), the laminar flow is linearly (centrifugally) unstable. In the co-rotating regime, the Rayleigh line ( $Re_i = Re_o/\eta^2$ ) is shown as blue, and is indistinguishable from the neutral stability curve at this scale. The black line ( $Re_i = Re_o/\eta$ ) indicates solid-body rotation, i.e. the flow has a constant angular velocity. Flows to the left of this line are anti-cyclonic, and cyclonic to the right. The grey line denotes exact counter-rotation (zero-mean rotation) and thus separates also cyclonic from anti-cyclonic regimes. (b) As in (a) but for the parameter space spanned by the shear Reynolds number  $Re_S$  and the rotation number  $R_\Omega$ , where exact rotation corresponds to  $R_\Omega = 0$ , the Rayleigh line to  $R_\Omega = -2$  and the solid-body line to  $R_\Omega \rightarrow -\infty$  from the anti-cyclonic side and  $R_\Omega \rightarrow -\infty$  from the cyclonic side.

In 2005, Dubrulle *et al.* [18] introduced an insightful alternative parametrisation of Taylor–Couette flow, which has improved our understanding of the physics of the system and embeds it in the wider context of rotating shear flows. They defined a shear Reynolds number ( $Re_S = 2/(1 + \eta)|Re_o\eta - Re_i|$ ) and a rotation number ( $R_\Omega = (1 - \eta)(Re_i + Re_o)/(Re_o\eta - Re_i)$ ), which measure the ratio of shear to viscous forces and the ratio of mean rotation to shear, respectively. Figure 1(b) shows the same diagram as discussed before, but in terms of  $R_\Omega$  and  $Re_S$ . This representation has the advantage that all the boundaries (except for the neutral stability curve) remain unchanged as  $\eta$  is varied. Crucially, the line for  $R_\Omega = 0$  (corresponding to exact counter-rotation/zero-mean rotation) separates cyclonic ( $R_\Omega > 0$ ) from anticyclonic ( $R_\Omega < 0$ ) flows and smoothly connects Taylor–Couette flow to rotating plane Couette flow in the limit of vanishing curvature,  $\eta \rightarrow 1$ . Hence, rotating plane Couette flow is just a specific (limiting) configuration of Taylor–Couette flow. Note that  $Re_S = 4Re$ , where  $Re$  is the usual Reynolds number for plane Couette flow, which is defined with the half-gap width and the wall velocity. The stability boundary derived by Rayleigh [7] for inviscid fluids (i.e., the Rayleigh line) is at  $R_\Omega = -2$ . Solid-body rotation can be approached from the cyclonic side ( $R_\Omega \rightarrow \infty$ ) or from the anticyclonic side ( $R_\Omega \rightarrow -\infty$ ). In  $(Re_o, Re_o)$ -space, however, these curves all depend on  $\eta$  and thus move around as the curvature of the system is varied. This makes the comparison of results obtained for different geometries more challenging.

Before discussing transition in the different regions, it is important to point out that all the curves shown in Fig. 1, as well as their stability properties, are defined/computed under the assumption of perfect laminar circular Couette flow. In experiments, this cannot be attained because of the end walls, which confine the flow in the axial direction and drive secondary flows. Hence, the aspect ratio  $\Gamma$  and the specific end-wall conditions used in experiments are additional important variables that need to be considered when comparing results from different Taylor–Couette simulations and experiments.



### 3. Supercritical route to turbulence

Taylor–Couette flow is least stable when the outer cylinder is held fixed, as noted early on by Mallock [6]. This specific configuration has attracted a lot of interest [19] because it simplifies the experimental setup considerably. In this section, we review the transition to turbulence for  $\eta = 0.875$  and stationary outer cylinder as  $Re_i$  is increased. Our choice is motivated by the influential experimental investigation of Gollub & Swinney [20], who measured time series of the radial velocity ( $u_r$ ) at mid gap and revealed three distinct instabilities, each adding a new frequency to the Fourier spectrum of  $u_r$  as  $Re_i$  was increased. In a further transition, the flow was shown to exhibit a continuous spectrum characteristic of chaotic dynamics, in apparent agreement with a theorem by Ruelle & Takens regarding the existence of chaotic dynamics near three-tori in dynamical systems [21]. In this section, we present new computational results to illustrate the transition process.

Periodic boundary conditions (BC) are employed in the axial ( $z$ ) and azimuthal ( $\theta$ ) directions and simulations are carried out using our pseudo-spectral DNS code **nsCouette** [22]. The highest friction Reynolds number ( $Re_\tau = u_\tau d/\nu$ ) measured in all DNS presented here is 95.7, where  $u_\tau$  is friction velocity at the inner cylinder wall. In all our DNS, the spatial resolution in terms of viscous units (i.e. in wall-units based on that  $Re_\tau$ ) is at least  $0.02 \leq \Delta r^+ \leq 1.3$ ,  $\Delta \theta r_i^+ = 3.8$  and  $\Delta z^+ = 3.5$ , which is state of the art in DNS of wall-bounded turbulence [23,24]. In **nsCouette**, the size of the time step is dynamically adapted during run time to ensure numerical accuracy and lies between  $5 \times 10^{-7}$  and  $5 \times 10^{-6}$  viscous time units,  $\frac{d^2}{\nu}$ , for all DNS shown (depending on the exact set-up). Except for the spiral turbulence simulation presented in §4(a), all DNS were run for at least 20 viscous time units, before data were recorded and analysed.

#### (a) Bifurcation cascade to temporal chaos

We begin by examining the onset of temporally chaotic dynamics in a small computational cell with axial aspect ratio  $\Gamma = \frac{5}{2}$  and only one quarter of the circumference in the azimuthal direction, i.e.,  $\theta \in [0, L_\theta]$  with  $L_\theta = \frac{\pi}{2}$ . This choice is made to match the sequence of patterns reported by Gollub & Swinney [20] for a system with  $\eta = \frac{7}{8}$  and  $\Gamma \approx 20$ . In their experiments, the primary instability took the form of Taylor vortices with a wavelength of approximately  $\frac{5}{2}d$ , corresponding to 8 vortex pairs in their apparatus. Our simulations are expected to capture the dynamics of the flow around the central section of the experiments, where the flow patterns are approximately periodic in the axial direction [20]. A summary of the flow patterns, dynamics and regimes as  $Re_i$  is increased in the simulations is presented in Fig. 2 and is explained in detail below.

At  $Re_i \approx 122$  circular Couette flow, C, becomes unstable and is replaced by a pair of axisymmetric Taylor vortices (TV), visualised in Fig 2(a) for  $Re_i = 150$ . In this transition, the invariance of C to axial translations is broken, while the rotational symmetry and the axial reflection symmetry (about the mid plane) are preserved. TV are time-independent, as can be seen in the time series of  $u_r$  recorded at mid gap position (Fig. 2(f)) and of the inner-cylinder Nusselt number  $Nu_i$  (Fig. 2(g)). The latter is the torque necessary to rotate the inner cylinder for a given flow state, normalised by the torque that would be required for circular Couette flow at the same Reynolds number.

Flow transitions, and more generally turbulence and transition, can be analysed from a dynamical systems perspective [25]. In this perspective, the Navier–Stokes equations span an infinite-dimensional phase space consisting of all admissible flow fields (satisfying mass and momentum conservation). Time-dependent flows correspond to trajectories in phase space and TV, which is time-independent, to a fixed point or steady state. The emergence of a new stable steady state (TV), which bifurcates from an existing one (C) that loses its stability, corresponds to a qualitative change in phase space or bifurcation. The bifurcation diagram in Fig. 2(e) captures this transition. Note that if TV is shifted axially by an arbitrary amount, the shifted TV pattern is still a solution to the system, so this bifurcation is known as a *pitchfork of revolution*. For a more detailed treatment, the reader is referred to [26] for an introduction to bifurcation theory, to [27]

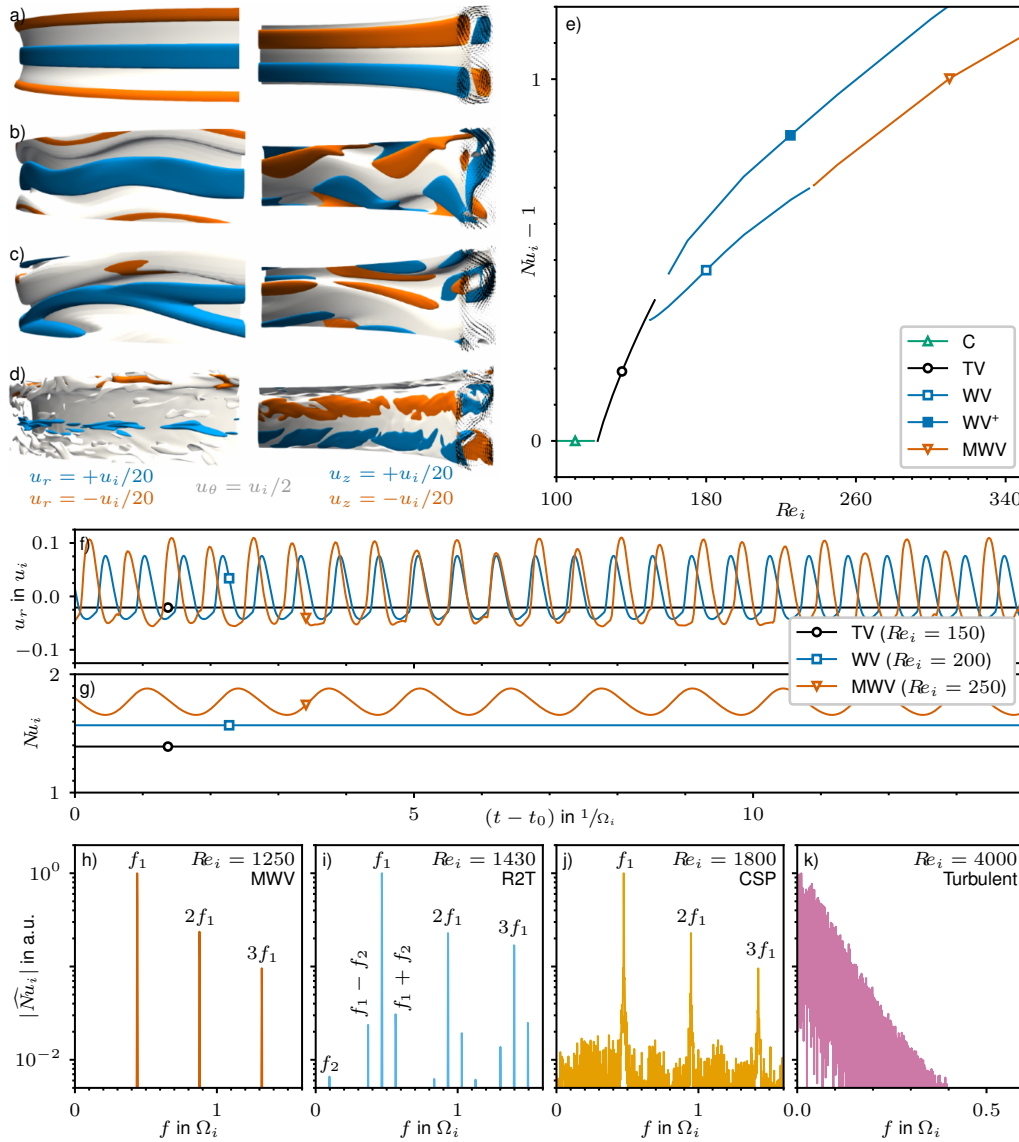


**Figure 2.** Route to turbulence in Taylor–Couette flow with a stationary outer cylinder as  $Re_i$  is increased from 100 to 4000 in DNS for  $\eta = \frac{7}{8}$ ,  $\Gamma = \frac{5}{2}$ , and  $L_\theta = \frac{\pi}{2}$ . (a)–(d) Visualisations of colour-coded iso-contours of the radial ( $u_r$ ), azimuthal ( $u_\theta$ ), and axial ( $u_z$ ) velocity components of the flow field, show that the spatial structure of the flow becomes progressively more complex as  $Re_i$  increases from (a)  $Re_i = 150$  (Taylor vortices, TV) to (b)  $Re_i = 200$  (wavy vortices, WV) to (c)  $Re_i = 250$  (modulated wavy vortices, MWV), and finally to (d)  $Re_i = 4000$  (turbulent flow). (e) Nusselt number of the inner cylinder ( $Nu_i$ ) as a function of  $Re_i$  for the flow states indicated in the legend. (f)–(g) Time series of  $u_r$  at mid gap and of  $Nu_i$  for selected flow states. (h)–(k) Power spectra of the time series of  $Nu_i$  for selected flow states; R2T is a relative two torus, CSP is a chaotic flow with a distinct dominant frequency.

for a discussion of equivariant bifurcation theory, to [28] for its application to Taylor–Couette flow, and to [29] for a review of symmetry-breaking bifurcations in fluid dynamics.

As the inner cylinder is further accelerated beyond  $Re_i \approx 150$ , TV turns unstable and the flow field becomes three-dimensional and time-dependent [16]. As shown in Fig. 2(b), the vortices acquire waviness in the azimuthal direction, breaking the rotational and the axial reflection

symmetry. However, if the pattern is rotated by  $\frac{\pi}{2}$  and reflected about the mid plane, it remains unchanged [30,31]. The time series of  $u_r$  for this wavy vortex (WV) state is now time-periodic (Fig. 2(f)). Generically, time-periodic states emerge from the loss of stability of steady states via Hopf bifurcations [26,32]. However, WV states are not truly periodic solutions, but rather rotating waves [33,34]. They rotate in  $\theta$  like a solid body, and as such the time-dependence disappears when integral measures such as the torque are considered (Fig. 2(g)). This is the reason why rotating waves are also known as relative equilibria [35]. We note that even for the small computational cell considered here, there exists at least one other wavy vortex solution (WV<sup>+</sup>) in the same parameter range. This is characterised by a higher Nusselt number (Fig. 2(e)).

Further increasing the Reynolds number beyond  $Re_i \approx 237$  leads to a modulated wavy vortex (MWV) state [33,36]. Now,  $u_r$  becomes quasi-periodic (Fig. 2(f)) and exhibits two independent frequencies, whereas  $Nu_i$  begins to oscillate periodically with frequency  $f_1$  (see the time series in Fig. 2(g) and the corresponding spectra in Fig. 2(h)). MWV are periodic orbits when seen in a frame moving at the speed of the underlying rotating wave [33] and hence are often referred to as relative periodic solutions [37]. At much larger Reynolds numbers ( $Re_i \approx 1429.69$ ), a new independent frequency ( $f_2$ ) becomes apparent in the spectrum of  $Nu_i$  (Fig. 2(i)), and the flow can be identified as a relative two torus (R2T) [38], i.e. a state with two independent frequencies ( $f_1$  and  $f_2$ ) when viewed in a co-moving frame. As  $Re_i$  is slightly increased (beyond  $Re_i \approx 1437.50$ ), R2T breaks down into chaos, as exemplified in the (turbulent) broadband spectrum for  $Re_i = 4000$  in Fig. 2(k). We note that we found other solutions in the parameter range studied here, notably a chaotic solution with a clearly dominant frequency,  $f_1$  in Fig. 2(j), is stable in wide parameter ranges. The computed flow states illustrate the dynamical richness of the Taylor–Couette system, and indeed many other flow states may exist. Exhausting the complete set of possible solutions (and the connections between them) is beyond the scope of this review article even for the small computational cell examined in this subsection.

The transition scenario observed in our simulations, including the Reynolds numbers of the instabilities, is in agreement with the experiments of Gollub & Swinney [20]. They stressed the remarkable resemblance of their experimental observations with the theory of Ruelle & Takens [21], who showed the existence of chaos close to three-frequency tori. However, as shown in Fig. 2(d), the flow state succeeding MVW is a relative two torus in a frame moving at the speed of the underlying rotating wave, and thus cannot directly break down into chaos [33]. Hence, their reported breakdown to chaos is actually in better agreement with a later paper by Newhouse, Ruelle & Takens [39], which demonstrated that generic breakdown to chaos is also possible from two tori. The resulting temporally chaotic flow initially retains spatial coherence in the azimuthal and axial directions, but this is gradually lost as  $Re_i$  is further increased further [40,41]. Nevertheless, large-scale structures called turbulent Taylor vortices (because of their similarity to TV) are observed to persist in the time-averages of turbulent flows up to the highest Reynolds numbers investigated so far ( $Re_S = \mathcal{O}(10^6)$ , [42]). The focus of this paper is on the transitional regime and the reader is referred to Grossmann *et al.* [43] for a review on turbulent Taylor–Couette flow.

## (b) Flows with defects

The results presented in the previous section were obtained using a small computational domain containing exactly one pair of Taylor vortices, TV, and one azimuthal wavelength of the wavy vortices WV. In the experiments [20], the WV repeated four times in the azimuthal direction and had eight pairs of vortices in the axial direction. This raises the question of whether the dynamics obtained in our small cell are also reproduced when spatially extended cells are considered. We carried out two DNS in a domain spanning the whole circumference and  $\Gamma = 25$ . The simulations were initialised with circular Couette flow, C, disturbed with a small perturbation repeating ten times in the axial direction and four times in the azimuthal direction, and numerical noise in the remaining modes. At  $Re_i = 200$ , C rapidly destabilised and ten pairs of TV formed, which subsequently developed into WV of the exact same periodicity as in the simulations of the

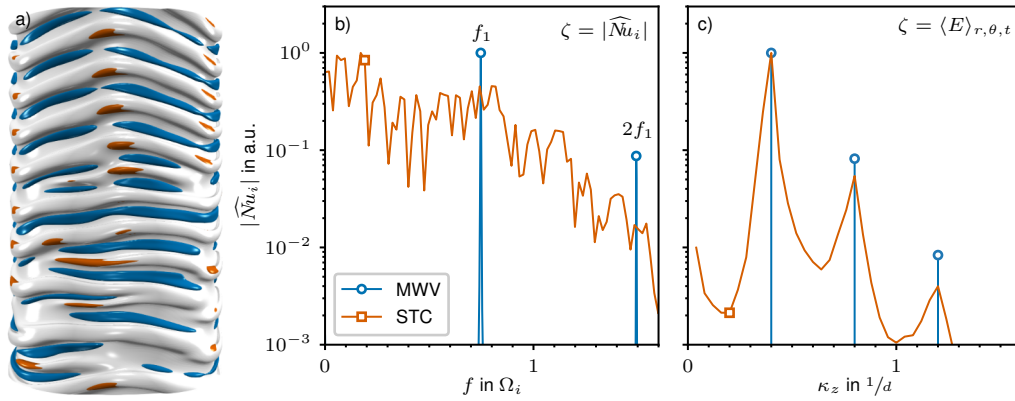


**Figure 3.** Spatio-temporal defects in large domains  $\Gamma = 25$ ,  $L_\theta = 2\pi$  obtained with DNS for  $\eta = \frac{7}{8}$  and  $Re_i = 250$ . (a) Visualisation of the flow state. Shown are colour-coded iso-surfaces of the velocity (white for  $u_\theta = u_i/2$  and red/blue for  $u_r = \pm u_i/20$ ). (b) Power spectra of the corresponding time series of  $\widehat{Nu}_i$  (red) compared to modulated wavy vortex (MWV) flow (blue) at  $Re_i = 250$  in a smaller domain with  $\Gamma = 5/2$  and  $L_\theta = \pi/2$  (i.e. the state shown in Fig. 2(c)). (c) Modal kinetic energy ( $\langle E \rangle_{r,\theta,t}(\kappa_z)$ ), where  $\kappa_z$  is the axial wave number.

previous section. An examination of the time series of  $u_r$  and  $\widehat{Nu}_i$  confirmed that indeed the computed flow state is identical in both cases.

At  $Re_i = 250$ , these two transitions were also observed and then followed by the transition to modulated wavy vortices, MVW, also exactly as in the previous section. However, after a very long time (20 viscous time units), the axial and azimuthal periodicity were lost as spatial defects appeared. A snapshot of this flow state is shown in Fig. 3(a). The temporal spectrum, shown in Fig. 3(b) as a red line, is continuous but features a broad, noisy peak close to the first harmonic of the spectrum of the MVW in the small domain (shown in blue). Similarly, all the spatial (axial) modes are excited, but as shown in Fig. 3(c), the spectrum exhibits a clearly dominant peak (and harmonics) corresponding to ten pairs of vortices. Detailed investigations of transitions to chaotic flows with spatial defects, often referred to as spatio-temporal chaos [44], are scarce and deserve more attention. One example was studied in magnetohydrodynamic Taylor–Couette flow, where the transition to defects was shown to emerge via a symmetry-breaking sub-harmonic bifurcation of a rotating wave [45]. While the temporal spectrum shown here is much noisier than that reported by Gollub & Swinney [20] for MVW, their spectrum also contains substantial noise. This may be due to the presence of defects in the flow, similar to those reported here, or to measurement errors, and cannot be clarified here. However, we point out that the end walls confining the fluid in the axial direction result in distinctly different bifurcations, as demonstrated e.g. in detailed experiments [46] and in DNS [47] for systems with moderate aspect ratios ( $\Gamma \sim 10$ ). End-wall effects in the linearly stable regime are reviewed below in § 3(d).

### (c) Flow patterns in the linearly unstable regime

The results discussed in the previous sections are specific to flows with a stationary outer cylinder and  $\eta = 7/8$ . Even for the small domain investigated in § 3(a), we found co-existence of many different states and other routes to chaos (not shown in detail here). This complexity is due to the nonlinear nature of the Navier–Stokes equations, resulting in a strong dependence on the initial conditions and in typical experiments on the path in  $(Re_o, Re_i)$ -space taken to prepare the system. This was known to Coles, who in his 1965 paper [16], reported that for a given flow configuration (i.e., pair of  $Re_i$  and  $Re_o$ ) there could be as many as 26 different possible stable flow

states (as characterised by their azimuthal and axial wavenumbers) with complicated dynamical connections between them.

When the cylinders are allowed to rotate independently in the linearly unstable region, extremely rich dynamics are found. This was beautifully illustrated by Andereck *et al.* [36], who extensively mapped out the two-dimensional parameter space spanned by  $(Re_i, Re_o)$  and revealed a large variety of flow regimes, characterised by their spatio-temporal symmetries, frequencies and azimuthal and axial wavenumbers. For example, in the counter-rotating regime, there exists a  $Re_o$ , at which the primary bifurcation to TV is replaced by a Hopf bifurcation to non-axisymmetric spiral vortices, which rotate in the azimuthal direction and travel along the axial direction. This spiral flow pattern was already observed by Taylor [1] in his seminal paper and was later studied in detail theoretically [48,49] and experimentally [50]. As the speed of inner cylinder is further increased, interpenetrating spiral patterns emerge and the flow later transitions to a chaotic state characterised by episodic bursts of turbulence superimposed on the laminar spirals [36,51–53]. This transition is just one of the multiple ones reported by [36] and many others thereafter [19]. The study of the various transitions between flow states has played a central role in the development of pattern formation theory [54,55].

#### (d) End-wall effects

Whether comparing results to the infinitely tall cylinders of theory, or to the periodic boundary conditions common to many simulations, the vertical boundaries of Taylor–Couette flow are a widespread source of limitation, but also of new phenomena. Mitigating their effects started early, for example with Mallock using a pool of mercury at the bottom of his cylinders as a buffer [56]. Accordingly the results discussed so far were for experiments with relatively tall cylinders  $\Gamma \gtrsim 20$  or DNS with periodic boundary conditions. Cole [57] systematically investigated the effect of varying  $\Gamma$  and observed that the critical Reynolds number for TV is in good agreement with theoretical predictions for infinite cylinders even for aspect ratios as low as  $\Gamma = 8$ . However, he found that  $\Gamma > 40$  was necessary to obtain quantitative agreement with axially periodic DNS regarding the rotation speed of WV.

From a theoretical stand point, the presence of end walls destroys the translation invariance of the system. In addition, the necessary discontinuity of the boundary conditions between end walls and inner/outer cylinder generates Ekman vortices [58]. As  $Re_i$  is increased, the cellular TV pattern first appears near the ends and rapidly fills the column when the system reaches the critical  $Re_i$  predicted for the infinite-cylinder case [57,59]. As a consequence, the transition to TV is not the result of a discrete bifurcation but is a continuous process [59].

In systems with the end-walls at rest and a stationary outer cylinder, the end-wall boundary layer tends to flow radially inward. However, Benjamin [59] found that cellular flows at low aspect ratio could also have an outflow at one or both end-wall boundary layers. These flows, termed anomalous modes, are disconnected in phase space from the circular Couette solution and appear only at higher  $Re_i$ . For  $\Gamma \sim 1$ , competition between the normal two-cell mode and the one-cell anomalous mode [60–62], along with the transition to chaos [63,64], have been extensively investigated. This specific case is particularly appealing for theoretical studies because the strong confinement drastically reduces the number of possible solutions to the Navier–Stokes equations. As the aspect ratio is increased, the temporal dynamics become increasingly complex and a multitude of local [46,47] and even global [65] bifurcations have been reported.

End-wall effects have been also investigated in the counter-rotating regime, albeit less intensively. Spirals can appear directly at the end walls and propagate toward the centre of the system below the critical Reynolds number predicted by the infinite-cylinder approximation [66]. The bifurcation scenario was found to depend strongly on the end-wall rotation speed [67]. Interpenetrating spirals have been also observed in recent experiments [68] and DNS [69] for  $\Gamma \sim 5$ , although the short aspect ratio results in a strongly modified laminar flow and a transition scenario that is qualitatively different from that observed for long cylinders [68].



## 4. Subcritical route to turbulence

The transition to turbulence in flows dominated by outer-cylinder rotation (the green region in Fig. 1) is of a completely different nature. For fixed parameters, one observes either laminar flow or spatio-temporally intermittent laminar-turbulent patterns. The absence of an instability cascade from laminar flow to states with increasing temporal complexity (e.g. TV, WV, MVW, etc.) greatly complicates the theoretical treatment of the transition to turbulence. As will be shown in this section, understanding the subcritical transition in linearly stable Taylor–Couette flow, and more generally in wall-bounded shear flows, requires stochastic approaches and additionally accounting for spatial effects. Neither of these two aspects is covered by the classical route to chaos demonstrated by Ruelle & Takens [21,39]. The appropriate framework to describe the subcritical transition to turbulence was first proposed by Kaneko [70], who extended the dynamical systems approach to linearly stable flows with co-existing turbulent and laminar domains. The first experimental studies embracing his spatio-temporal perspective were carried out in the nineties by Bottin *et al.* [14,71] for plane Couette flow.

### (a) Spiral turbulence and turbulent spots

Mallock [6] noted that in flows with stationary inner cylinder and rapid outer cylinder rotation, “When the velocity approached that at which instability was liable to occur, it was interesting to notice how small a disturbance of the system was sufficient to change the entire character of the motion. A slight blow on the support which carried the apparatus, or a retardation for a few moments of the rotation of the outer cylinder, was almost sure to produce the effect.” The flow patterns emerging from the transition consist of well-defined turbulent domains (spots) that evolve in an otherwise laminar background, as reported by Reynolds for pipe flow [3]. Coles [16] observed that individual spots sometimes spontaneously laminarised, but could also grow in size and sometime merge with other spots. He reported that under some conditions turbulent spots came together and formed a spiral band of turbulence that cork-screwed around the apparatus, see Fig. 4(a)–(b). The eminent physicist Richard Feynman, who was a Professor at Caltech at the same time as Coles, was intrigued by the origin of this surprisingly organised, but at the same time turbulent pattern, which he called “barber-pole turbulence” [72].

The emergence of spiral turbulence is demonstrated in the second row of Fig. 4, which shows snapshots from the experiments of Burin & Czarnocki [73] in a system with a stationary inner cylinder and  $\eta = 0.97$ . In these snapshots and in the corresponding supplementary movie, laminar regions gradually appear as  $Re_o$  is decreased and lead to the formation of the laminar-turbulent spiral pattern, with one helicity dominating after an initial mixed-helicity phase. This transition process has been modelled as a long-wave instability of the turbulent flow [74]. As  $Re_o$  is further decreased, the spiral turbulence retains its form (although spirals of opposite helicity may appear), until it begins to progressively disintegrate into spots. These spots are sometimes elongated, in line with the spiral angle, and their boundary appears to propagate in this direction as well (see e.g., the video at  $Re_o = 2100$ ). Finally, the flow laminarises fully at sufficiently low  $Re_o \approx 2000$ .

The laminarisation boundary of turbulent spots has been measured by many authors experimentally [14–16,36,52,53,73,76] and in DNS [52,78,79]. These measurements are summarised in Fig. 5, where the lowest  $Re_S$  for turbulence survival is shown as a function of  $R_\Omega$ . Recall that  $R_\Omega = 0$  corresponds to exact counter-rotation and the first measurement point here corresponds to plane Couette flow, with  $Re_S \approx 1300$  [14]; recall that  $Re_S = 4Re$ , where  $Re$  is the Reynolds number commonly defined for plane Couette flow. This is followed by the experiments of Klotz *et al.* for extremely narrow gap ( $\eta = 0.997$ ) and stationary inner cylinder, with  $Re_S \approx 1320$  and  $R_\Omega = 0.003$ . As  $R_\Omega$  is increased and cyclonic rotation is added, higher  $Re_S$  is required to sustain turbulence. As shown in Fig. 5, experimental data from various studies collapse well into a single curve despite the wide ranges covered in curvature  $\eta \in [0.789, 1]$  and in Reynolds numbers ( $Re_i \in [-1000, 1200]$  and  $Re_o \in [-50000, -1200]$ ). One exception to this are the transition points



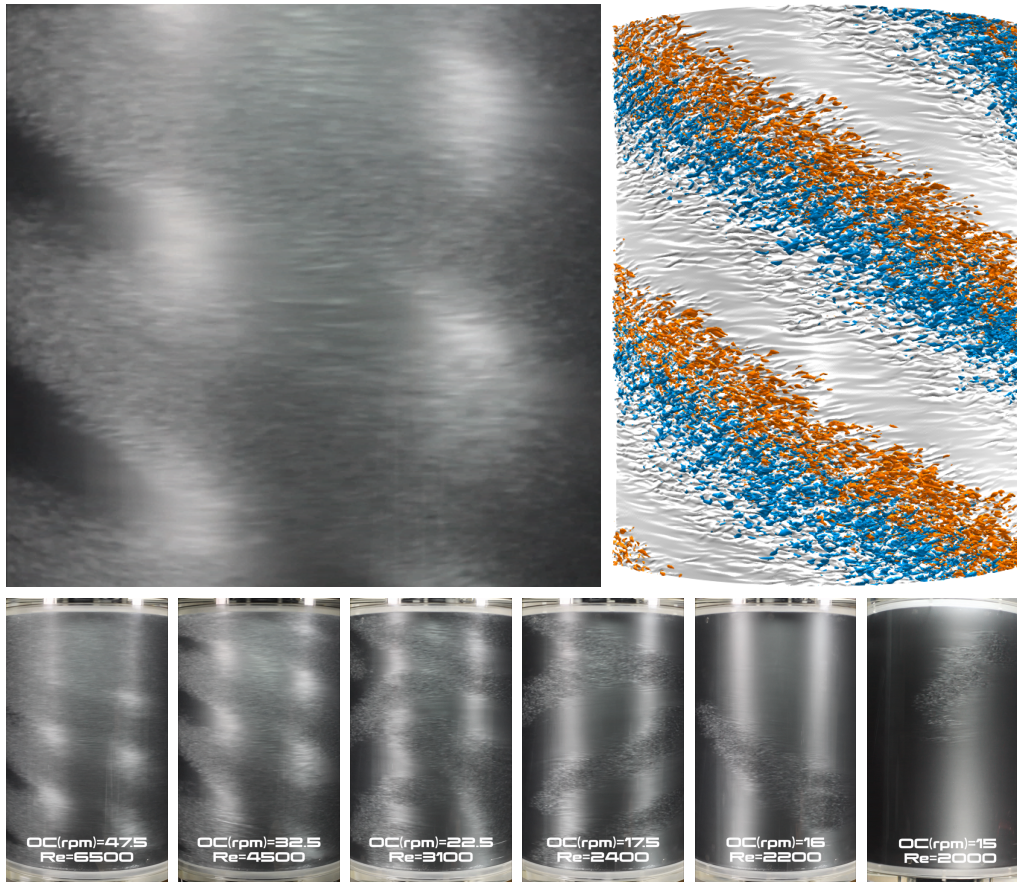


**Figure 4.** (a)–(b) Spiral turbulence in experiments [73] and DNS for a stationary inner cylinder in a system with  $\eta = 0.97$  at  $Re_o = 4500$ . In the experiments,  $\Gamma = 92$  and Kalliroscope flakes were added to the water for imaging. In the DNS, periodic periodic boundary conditions in  $\theta$  and  $z$  were used in a computational cell with  $\Gamma = 61.3$  and  $L_\theta = \pi/2$ . Shown are colour-coded iso-contours for  $u_\theta = Re_o/2$  (light grey) and  $u_r = \pm Re_o/10$  (red/blue). (c) Sequence of flow patterns as  $Re_o$  is decreased in the experiments from  $Re_o = 6500$  to  $2000$  (Supplementary video online).

obtained by Burin & Czarnocki [73] for wide gaps,  $\eta = 0.73$  and  $0.55$  (the latter not shown in the figure). For a fixed experimental apparatus, wider gaps mean lower  $\Gamma$ , which combined with the increased  $Re_S$  required for subcritical transition leads to end-wall effects being very significant. These end-effects greatly perturb the primary flow and may trigger subcritical transition [73] or even result in linear instabilities [80–82].

The collapse of the data illustrate the suitability of the parametrisation introduced by Dubrulle *et al.* [18] and demonstrate that the specific case of stationary outer cylinder (with  $R_\Omega = 1/\eta - 1$ ) does not exhibit some form of singularity, as Fig. 1(a) may initially suggest. This point is further confirmed by the experiments of Coles [16], who continued the laminarisation curve from the counter-rotating to the co-rotating regime. Note also that curvature influences the laminarisation boundary only indirectly through  $R_\Omega$ , at least up to  $\eta \gtrsim 0.789$  as shown by the experiments of Litschke & Roesner [76].

Extending measurements to larger  $R_\Omega$  would be valuable, but is challenging. Specifically, as  $R_\Omega$  increases,  $Re_S$  grows exponentially, necessarily resulting in a huge difference between the angular speeds of the inner and outer cylinders. This exacerbates end-wall effects in experiments and has extremely high computational cost in axially periodic DNS. Finally, we stress that while

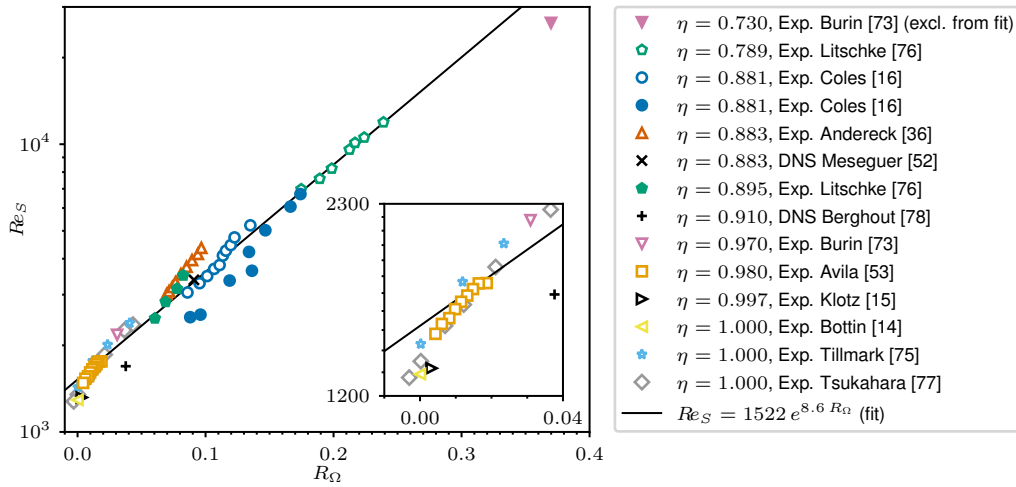


**Figure 5.** Critical shear Reynolds number  $Re_S$  as a function of rotation number  $R_\Omega$  for experiments [14–16,36,53,73,75–77] and DNS [52,78]. The data span a wide range of gaps,  $\eta \in [0.73, 1]$  and Reynolds numbers  $Re_i \in [-1000, 1200]$  and  $Re_o \in [-50000, -1200]$ . Most measurements were taken in the subcritical counter-rotating regime (the region below the linear stability boundary for  $Re_o < 0$  in Fig. 1(a)), including the case of stationary inner cylinder  $Re_i = 0$ . Coles [16] also performed measurements in the cyclonic co-rotating regime.

the boundary at which turbulence can become sustained depends only on the system parameters, the natural (uncontrolled) transition boundary, where turbulence is observed to appear as  $Re_S$  is increased, depends on the level of disturbance present in the experiment and can vary by as much as one order of magnitude in  $Re_S$  for the same geometry and  $R_\Omega$  [83].

### (b) Transient turbulence: stochastic decay of turbulent spots

The experiments reported by Mallock [6], Taylor [11] and Coles [16] demonstrated that, once triggered, turbulent episodes can last almost indefinitely or relaminarise after irregular intervals. This essentially implies that the lower boundary discussed in the previous section depends on the observation time and on the experimental realisation. This explains in part the scatter in Fig. 5.

The first systematic study of the stochastic nature of turbulence decay in Taylor–Couette flow was performed in 2010 by Borrero-Echeverry *et al.* [84]. They investigated a system driven by pure outer cylinder rotation and repeated experiments up to 1200 times at a single  $Re_o$  to statistically characterise the duration of turbulent episodes. Their visualisations indicated that turbulence collapses suddenly and without warning. The duration (or lifetime) of turbulence in each experimental run is shown in Fig. 6(a) for  $Re_o = 8106$ . The corresponding lifetime distribution, shown in (b), is exponential. This implies that turbulence relaminarisation follows a memoryless process, exactly as reported earlier for plane Couette [14] and pipe flows [85,86]. By collecting distributions at various  $Re_o$ , Borrero *et al.* showed that the associated time constant  $\tau_d$  (the average lifetime) increases super-exponentially with  $Re_o$ , but remains finite as  $Re_o$  increases. This result, in qualitative agreement with previous studies of pipe flow [87,88], was confirmed by Alidai *et al.* [89], who additionally showed that the typical lifetime of turbulent episodes does not depend on the specific details of how the turbulence is initially triggered, but is significantly affected by imperfections in the experimental apparatus, and by the end-wall conditions. Finally, they also showed that as the aspect ratio of the system is reduced,  $\tau_d$  decreases.

Goldenfeld *et al.* [90] proposed that turbulent spots relaminarise when all turbulent fluctuations within the spot fall below a certain level. With this assumption they exploited extreme-value theory, where super-exponential scaling appears as a matter of course [91], to

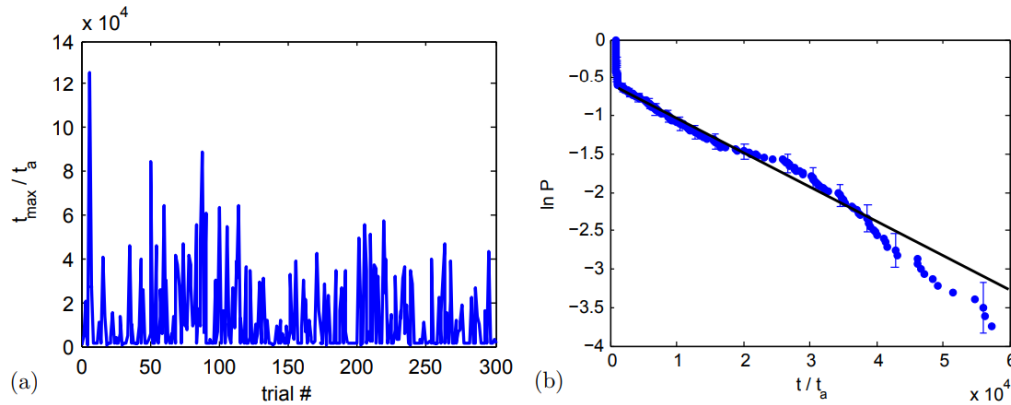


**Figure 6.** (a) Duration,  $t_{max}$ , of turbulent episodes in Taylor–Couette flow with  $\eta = 0.871$ ,  $\Gamma = 33.6$ ,  $Re_o = 8106$  and  $Re_i = 0$ . Turbulence is triggered by briefly counter-rotating the inner cylinder. For some runs turbulence collapses almost immediately, but for others it persists for long times. (b) The probability  $P$  that turbulence survives up to time  $t$  decays exponentially with rate  $1/\tau_d$ , the slope of the exponential tail on the semi-log scale, where  $\tau_d$  is the average survival time. Also visible is a fraction of experimental runs that do not become turbulent (highlighted by the almost vertical drop in  $P$  near  $t = 0$ ). All times are reported in advective time units  $t_a = \frac{d}{r_o \Omega_o}$ . The error bars in (b) represent sampling error and are shown at representative points.

develop a model consistent with the scaling of  $\tau_d$  observed in experiments [84,87]. This idea has recently been tested and elaborated further in DNS studies [92,93].

### (c) Onset of sustained turbulence: spatio-temporal proliferation of spots

Despite the transient nature of individual turbulent spots, Moxey & Barkley [94] showed a mechanism by which the proliferation of turbulent puffs can lead to sustained turbulence in pipe flow. Avila *et al.* [95] further showed that the probability of a spot to grow and shed a daughter one, statistically identical to its parent, increases as the Reynolds number increases. Specifically, the associated proliferation time constant decreases super-exponentially with Reynolds number. The competition between the stochastic processes of turbulence decay and turbulence proliferation determines the critical Reynolds number for the onset of sustained turbulence in pipe flow [95]. The same mechanism was later demonstrated in a narrow-gap Taylor–Couette system [96], in which the computational cell was spatially extended in one direction only (as happens naturally in pipe flow).

Beyond the critical point, turbulence proliferates faster than it decays and the fraction of the experiment occupied by turbulence increases with the Reynolds number. This was explicitly demonstrated by Lemoult *et al.* [97], who precisely measured the evolution of the turbulence fraction as a function of  $Re_o$  for a system with stationary inner cylinder and very narrow gap,  $\eta = 0.998$ . Their short aspect ratio ( $\Gamma = 8$ ) allowed turbulence to localise only in the azimuthal direction, whilst filling the apparatus in the axial direction. The turbulence fraction was found to increase continuously from zero at the critical point, corresponding to a second-order phase transition. The spatio-temporal dynamics of the turbulent spots, and of the laminar gaps between them, could be shown to fall into the universality class of directed percolation, which is the simplest case of a non-equilibrium phase transition. We stress that in this system the dynamics of spots is exactly as in pipe flow due to the axial confinement. The critical exponents could be accurately determined with extremely long measurement times, because Taylor–Couette flow is a closed system (in contrast to pipe flow, where turbulent puffs ultimately leave the pipe at its downstream end).

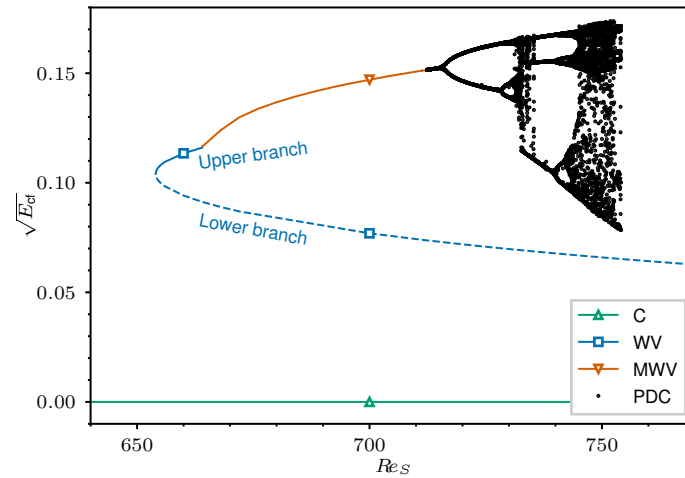


**Figure 7.** Bifurcation diagram showing the onset of chaotic transients in plane Couette flow in a small, symmetry-restricted cell. The kinetic energy contained in the cross-flow velocity components,  $\sqrt{E_{cf}}$ , is shown as a function of the shear Reynolds number,  $Re_S$ . A pair of steady wavy vortex (WV) solutions is born at a saddle-node bifurcation at  $Re_S \approx 655$ . The upper branch is stable in the symmetry-restricted space, but loses stability in a Hopf bifurcation to a modulated wavy vortex (MWV) state at  $Re_S \approx 664$ . Subsequently, a period-doubling cascade (PDC) generates a chaotic attractor, although there is a short window ( $735 < Re_S < 740$ ) with a stable period three state. The chaotic attractor is destroyed at  $Re_S \approx 754$  and thereafter all trajectories laminarise. Note, that the shear Reynolds number is related to the usual plane Couette Reynolds number as  $Re_S = 4Re$ . The data shown in this figure is replotted with permission from [102].

It is worth noting that the mechanisms of turbulent proliferation are qualitatively different in flows extended in one and in two directions. In the former, the turbulence fraction can only increase as the spots grow in the azimuthal direction, whereas in the latter spots can also extend in the axial direction. In both cases the transition is of second order [98]. What's more, recent measurements with  $\eta = 0.997$  and very tall cylinders  $\Gamma = 750$  [15] exhibit also a directed percolation transition, but with the exponents for systems extended in two directions (here axial and azimuthal). The interested reader is referred to [99] for a review about laminar-turbulent patterns in wall-bounded flows extended in two spatial directions.

#### (d) Simple invariant solutions and the origin of transient turbulence

The results discussed in the previous section resolve the question of the onset of sustained turbulence in linearly unstable flows, but do not provide information as to how chaotic dynamics appears in the phase space of the system. In an influential paper, Nagata [100] showed in 1990 that a specific wavy vortex solution, similar to the WV shown in Fig. 2(b) for stationary outer cylinder, could be numerically continued from Taylor–Couette to plane Couette flow (without rotation). In this limit, the WV solution remains three-dimensional, but becomes steady. More importantly, it is disconnected from the laminar (plane) Couette flow in phase space, a result that holds already for very narrow gap Taylor–Couette flow,  $\eta \gtrsim 0.993$ , [101]. In other words, in plane Couette flow there is no sequence of instabilities leading from laminar flow to WV because the laminar flow is linearly stable. Nagata's remarkable discovery paved the way for applying the dynamical-systems approach to linearly stable flows.

At the lowest Reynolds number (called saddle-point) at which Nagata's WV solution exists, it is stable in a certain symmetry-restricted subspace (but unstable in full space). As shown in Fig. 7 (data replotted with permission from [102]), at Reynolds numbers slightly above the saddle-point this solution undergoes a Hopf bifurcation leading to a periodic solution [103]. This is exactly as the bifurcation into a relative periodic solution (MWV) from WV shown earlier in Fig. 2. As

the Reynolds number is further increased, a period-doubling cascade renders the flow chaotic. Despite the difference in the precise bifurcations occurring here and in the case shown earlier in the bifurcation diagram of Fig. 2(e), the situation is similar in both cases. Chaos emerges from a simple solution (WV) after a short bifurcation sequence during which symmetries are lost and the temporal complexity increases. We however stress that in plane Couette flow, these changes in phase space occur far away from the laminar flow, which actually remains stable to infinitesimal disturbances for all  $Re_S$  [104].

As  $Re_S$  is further increased, the chaotic attractor's volume grows in phase space, i.e. larger fluctuations of the velocity occur. Finally, the attractor collides with a twin lower branch WV solution, born at the same saddle-node bifurcation, and is destroyed [105]. Beyond this  $Re_S$  the chaotic dynamics is not sustained, but transient, and the resulting lifetime distributions are exponential [106]. Although this is consistent with the experimental observations at larger  $Re_S$  described in the previous section, there are crucial qualitative differences. The DNS described in this section were performed by imposing artificial symmetries in small computational cells. This stabilises the solutions, simplifies the temporal dynamics and precludes the spatial localisation typical of turbulent spots. In conclusion, a wide gap between theory and experiment remains at this stage. The interested reader is referred to the recent review by Avila *et al.* [9] (with main focus on pipe flow).

Several families of simple solutions with distinct symmetries have been computed in Taylor–Couette flow to date [107–109]. A particularly interesting solution computed for plane Couette flow [110] is spatially localised in the form of a spiral, similar to the spiral turbulence observed in experiments and shown in Fig. 4. Generally, these solutions are all unstable, but it has been demonstrated that the phase space of the turbulent dynamics is organised around them and their stable and unstable manifolds [111,112]; see [113,114] for recent reviews. More recent studies using a Taylor–Couette system with  $\Gamma = 1$  have provided experimental evidence supporting the importance of simple solutions in organising the turbulent dynamics [115–117].

We conclude this section by noting that Deguchi [118] recently made the surprising discovery of a linear instability of Taylor–Couette flow with stationary inner cylinder. However, for typical experimental gap widths ( $\eta \gtrsim 0.1$ ), this instability occurs at extreme Reynolds numbers,  $Re_o \gtrsim 10^7$ ). Even if these numbers could be attained in experiments (not achieved so far), subcritical transition would certainly occur well before the instability could be observed.

## 5. Keplerian regime

Of particular interest in recent years is the so-called quasi-Keplerian regime, with  $-2 < R_\Omega < -1$ , for its potential relevance to astrophysical disks. Astronomers infer that the outward transport of angular momentum needed for observed accretion rates takes place via disk turbulence, and the origin of this turbulence has generated considerable discussion, especially for cooler disks where the gas is largely neutral and the ambient magnetism may not play a significant dynamical role [119]. Orbiting shear flows naturally result from gravitation around a centralised mass, and while an exact Keplerian profile (with  $\Omega(r) \propto r^{-3/2}$ ), cannot be created in traditional Taylor–Couette flow, quasi-Keplerian (QK) flows (see the green region in Fig. 1) have generated interest in addressing the origin of disk turbulence. This flow regime is linearly stable and anti-cyclonic, featuring opposing gradients of radially decreasing angular velocity and radially increasing angular momentum. For ordinary (non-conducting) isothermal fluids, any transition is expected to be subcritical. However, we point out that results from the subcritical cyclonic regime discussed in the previous section do not offer much guidance for the anti-cyclonic QK regime.

For almost two decades, experiments in the QK regime presented conflicting results. Ji *et al.* [120], used two-dimensional laser Doppler velocimetry (LDV) to demonstrate that a quiescent flow is maintained even up to  $Re_S = 2 \times 10^6$ , which was at the limit of their experimental apparatus. It was then surmised that disks were hydrodynamically stable. However, the opposite conclusion, at slightly lower  $Re_S$ , was reached by Paoletti & Lathrop [121] using torque measurements as an integral measure of the angular momentum transport. In both



experiments considerable care was taken to minimise end-wall effects, with Ji *et al.* utilising split, independently-rotating end-caps and Paoletti & Lathrop measuring torque on the central portion of the inner cylinder only.

The influence of end-wall effects has remained an epicentre of discussion and disagreement, but the problem has come into better focus more recently. Further experiments where a high  $Re_S$  quasi-Keplerian flow was actively perturbed, clearly demonstrated stability [122], i.e., laminar flow at high  $Re_S$ , bolstering the earlier result [120]. Direct numerical simulations [81,123] brought clarity to the apparently conflicting experimental results in detailing how boundary effects can be significant even at moderate  $Re_S$ . Specifically, if the end-wall conditions are carefully chosen, turbulence becomes confined to thin boundary layers as  $Re_S$  increases, while the bulk flow remains laminar. For additional elaboration on this topic, including stratification and magnetic effects, we refer to the review by Ji & Goodman in this centennial volume.

## 6. Conclusion

Starting with Taylor's groundbreaking work, Taylor–Couette flow has become the archetype to study hydrodynamic stability, bifurcations, pattern formation and transition to turbulence. More generally, the development of the dynamical systems framework to study dissipative systems has been greatly inspired and influenced by experimental observations of the system. The detailed bifurcation mechanisms and features of the flow patterns depend sensitively on the four dimensionless control parameters of the problem ( $Re_i$ ,  $Re_o$ ,  $\eta$ ,  $\Gamma$ ), and of the axial boundary conditions. As a consequence, the dynamical richness of Taylor–Couette flow has no limits and in this review we only summarised briefly some of the main traits.

Despite qualitative differences in the instabilities and flow patterns preceding turbulence, the transition to turbulence falls into one of two main categories, which we termed supercritical and subcritical. The first one is characterised by a sequence of bifurcations eventually leading to temporally chaotic dynamics. The ensuing flow patterns fill the whole apparatus and sequentially lose spatial symmetry and coherence. These bifurcations were studied experimentally, numerically and theoretically in great detail in the last century. The catastrophic, subcritical route to turbulence was also studied and characterised experimentally back then, but it is only in the last two decades that an understanding of the underlying mechanisms has emerged. This has been possible thanks to statistically resolved spatio-temporal characterisations of very large systems up to extremely long times. The two key physical mechanisms underlying the directed-percolation transition to sustained turbulence in linearly stable Taylor–Couette flow are turbulence decay and proliferation. Both are stochastic processes. In the counter-rotating regime, things become even more complicated as the linearly unstable layer close to the inner cylinder interacts with the linearly stable (but nonlinearly unstable) one close to the outer cylinder. This results in a mixture of the two transition routes and is a topic that deserves more attention. It is not only relevant to Taylor–Couette flow, but also to e.g. curved pipes [124].

A third, perhaps even more intriguing case is the absence of turbulence and hence of a route to it. In the quasi-Keplerian regime, the weight of the experimental evidence suggests that circular Couette flow is stable up to at least  $Re_S = \mathcal{O}(10^6)$ . Whether transition occurs at even higher Reynolds numbers remains an outstanding question. The exponential stabilisation of circular Couette flow revealed here for the cyclonic regime cannot be extrapolated to the anti-cyclonic regime, but highlights the efficiency of system rotation in undermining the regeneration mechanisms of wall-bounded turbulent flows.

**Data Accessibility.** The data presented here will be provided in an online supplement (**Pangaea**) upon approval for publication. Data and code is additionally available here **nsCouette**.

**Authors' Contributions.** D. Feldmann designed/performed the simulations, analysed the data, and created Figs. 1–5, 4. M. Avila designed/coordinated the research, analysed the data and wrote the first draft. D. Borrero-Echeverry conducted the experiments and analysed the data presented in Fig. 6. All authors edited and approved the manuscript.

**Competing Interests.** The authors declare that they have no competing interests.



**Funding.** D. F. and M. A. gratefully acknowledge financial support from the German Research Foundation (DFG) through the priority programme [Turbulent Superstructures \(SPP1881\)](#) and computational resources provided by the [North German Supercomputing Alliance \(HLRN\)](#) through project hbi00041.

**Acknowledgements.** The authors would like to thank T. Kreilos for providing the data presented in Fig. 7

## References

1. Taylor GI. 1923 VIII. Stability of a viscous liquid contained between two rotating cylinders. *Philosophical Transactions of the Royal Society of London. Series A, Containing Papers of a Mathematical or Physical Character* **223**, 289–343.
2. Eckert M. 2010 The troublesome birth of hydrodynamic stability theory: Sommerfeld and the turbulence problem. *The European Physical Journal H* **35**, 29–51.
3. Reynolds O. 1883 An experimental investigation of the circumstances which determine whether the motion of water shall be direct or sinuous, and of the law of resistance in parallel channels. *Philosophical Transactions of the Royal Society of London. Series A, Containing Papers of a Mathematical or Physical Character* **174**, 935–982.
4. Orr WM. 1907 The stability or instability of the steady motions of a perfect liquid and of a viscous liquid. Part II: A viscous liquid. *Proceedings of the Royal Irish Academy. Section A: Mathematical and Physical Sciences* **27**, 69–138.
5. Sommerfeld A. 1909 Ein Beitrag zur hydrodynamischen Erklärung der turbulenten Flüssigkeitsbewegung. In *Proceedings of the 4th International Mathematical Congress, Rome 1908* vol. 3 pp. 116–124.
6. Mallock A. 1896 Experiments on Fluid Viscosity. *Philosophical Transactions of the Royal Society of London. Series A, Containing Papers of a Mathematical or Physical Character* **1897**, 41–56.
7. Rayleigh, Lord. 1917 On the dynamics of revolving fluids. *Proceedings of the Royal Society of London. Series A, Containing Papers of a Mathematical and Physical Character* **93**, 148–154.
8. Couette M. 1890 Distinction de deux régimes dans le mouvement des fluides. *Journal de Physique Théorique et Appliquée* **9**, 414–424.
9. Avila M, Barkley D, Hof B. 2023 Transition to Turbulence in Pipe Flow. *Annual Review of Fluid Mechanics* **55**, in press.
10. Wendt F. 1933 Turbulente Strömungen zwischen zwei rotierenden konaxialen Zylindern. *Ingenieur-Archiv* **4**, 577–595.
11. Taylor GI. 1936 Fluid Friction Between Rotating Cylinders I – Torque Measurements. *Proceedings of the Royal Society of London. A. Mathematical and Physical Sciences* **157**, 546–564.
12. Barkley D. 2016 Theoretical perspective on the route to turbulence in a pipe. *Journal of Fluid Mechanics* **803**.
13. Daviaud F, Hegseth J, Bergé P. 1992 Subcritical transition to turbulence in plane Couette flow. *Physical Review Letters* **69**, 2511–2514.
14. Bottin S, Chaté H. 1998 Statistical analysis of the transition to turbulence in plane Couette flow. *The European Physical Journal B* **6**, 143–155.
15. Klotz L, Lemoult G, Avila K, Hof B. 2022 Phase Transition to Turbulence in Spatially Extended Shear Flows. *Physical Review Letters* **128**, 014502.
16. Coles D. 1965 Transition in circular Couette flow. *Journal of Fluid Mechanics* **21**, 385–425.
17. Maretzke S, Hof B, Avila M. 2014 Transient growth in linearly stable Taylor–Couette flows. *Journal of Fluid Mechanics* **742**, 254–290.
18. Dubrulle B, Dauchot O, Daviaud F, Longaretti P, Richard D, Zahn J. 2005 Stability and turbulent transport in Taylor–Couette flow from analysis of experimental data. *Physics of Fluids* **17**.
19. Tagg R. 1994 The Couette–Taylor Problem. *Nonlinear Science Today* **4**, 1–25.
20. Gollub JP, Swinney HL. 1975 Onset of turbulence in a rotating fluid. *Physical Review Letters* **35**, 927.
21. Ruelle D, Takens F. 1971 On the Nature of Turbulence. *Communications in Mathematical Physics* **20**, 167–192.
22. López JM, Feldmann D, Rampp M, Vela-Martín A, Shi L, Avila M. 2020 nsCouette–A high-performance code for direct numerical simulations of turbulent Taylor–Couette flow. *SoftwareX* **11**, 100395.
23. Ostilla-Mónico R, Verzicco R, Grossmann S, Lohse D. 2016 The near-wall region of highly turbulent Taylor–Couette flow. *Journal of Fluid Mechanics* **788**, 95–117.

24. Feldmann D, Morón D, Avila M. 2021 Spatiotemporal intermittency in pulsatile pipe flow. *Entropy* **23**, 1–19.
25. Hopf E. 1948 A mathematical example displaying features of turbulence. *Communications on Pure and Applied Mathematics* **1**, 303–322.
26. Kuznetsov YA. 2004 *Elements of Applied Bifurcation Theory, Third Edition*. Number 112 in Applied Mathematical Sciences. New-York: Springer-Verlag third edition.
27. Chossat P, Lauterbach R. 2000 *Methods in Equivariant Bifurcations and Dynamical Systems*. World Scientific.
28. Chossat P, Iooss G. 1994 *The Couette-Taylor problem*. Berlin, Germany: Springer-Verlag.
29. Crawford JD, Knobloch E. 1991 Symmetry and symmetry-breaking bifurcations in fluid dynamics. *Annual Reviews of Fluid Mechanics* **23**, 341–387.
30. Marcus PS. 1984 Simulation of Taylor-Couette flow. Part 2. Numerical results for wavy-vortex flow with one travelling wave. *Journal of Fluid Mechanics* **146**, 65–113.
31. Wereley ST, Lueptow RM. 1998 Spatio-temporal character of non-wavy and wavy Taylor-Couette flow. *Journal of Fluid Mechanics* **364**, 59–80.
32. Hopf E. 1942 Abzweigung einer periodischen Lösung von einer stationären Lösung eines Differentialsystems. *Ber. Math.-Phys. Kl Sächs. Akad. Wiss. Leipzig* **94**, 1–22.
33. Rand D. 1982 Dynamics and Symmetry. Predictions for Modulated Waves in Rotating Fluids. *Archive for Rational Mechanics and Analysis* **79**, 1–37.
34. King GP, Li Y, Lee W, Swinney HL, Marcus PS. 1984 Wave speeds in wavy Taylor-vortex flow. *Journal of Fluid Mechanics* **141**, 365–390.
35. Krupa M. 1990 Bifurcations of relative equilibria. *SIAM Journal on Mathematical Analysis* **21**, 1453–1486.
36. Andereck CD, Liu SS, Swinney HL. 1986 Flow regimes in a circular Couette system with independently rotating cylinders. *Journal of Fluid Mechanics* **164**, 155–183.
37. Viswanath D. 2007 Recurrent motions within plane Couette turbulence. *Journal of Fluid Mechanics* **580**, 339–358.
38. Wulff C, Lamb JSW, Melbourne I. 2001 Bifurcation from relative periodic solutions. *Ergodic Theory and Dynamical Systems* **21**, 605–635.
39. Newhouse S, Ruelle D, Takens F. 1978 Occurrence of strange Axiom A attractors near quasi periodic flows on  $T^m$ ,  $m \geq 3$ . *Communications in Mathematical Physics* **64**, 35–40.
40. Brandstätter A, Swinney HL. 1987 Strange attractors in weakly turbulent Couette-Taylor flow. *Physical Review A* **35**, 2207–2220.
41. Lathrop DP, Fineberg J, Swinney HL. 1992 Transition to shear-driven turbulence in Couette-Taylor flow. *Physical Review A* **46**, 6390–6405.
42. Huisman SG, Van Der Veen RC, Sun C, Lohse D. 2014 Multiple states in highly turbulent Taylor-Couette flow. *Nature communications* **5**, 1–5.
43. Grossmann S, Lohse D, Sun C. 2016 High-Reynolds Number Taylor-Couette Turbulence. *Annual Reviews of Fluid Mechanics* **48**, 53–80.
44. Cross M, Hohenberg P. 1994 Spatiotemporal chaos. *Science* **263**, 1569–1570.
45. Guseva A, Willis A, Hollerbach R, Avila M. 2015 Transition to magnetorotational turbulence in Taylor-Couette flow with imposed azimuthal magnetic field. *New Journal of Physics* **17**, 093018.
46. Abshagen J, von Stamm J, Heise M, Will C, Pfister G. 2012 Localized modulation of rotating waves in Taylor-Couette flow. *Physical Review E* **85**, 056307.
47. Lopez JM, Marques F. 2015 Dynamics of axially localized states in Taylor-Couette flows. *Physical Review E* **91**, 053011.
48. Krueger ER, Gross A, Di Prima RC. 1966 On the relative importance of Taylor-vortex and non-axisymmetric modes in flow between rotating cylinders. *Journal of Fluid Mechanics* **24**, 521–538.
49. Langford WF, Tagg R, Kostelich EJ, Swinney HL, Golubitsky M. 1988 Primary instabilities and bicriticality in flow between counter-rotating cylinders. *Physics of Fluids* **31**, 776–785.
50. Snyder HA. 1968 Stability of rotating Couette flow. I. Asymmetric waveforms. *Physics of Fluids* **11**, 728–734.
51. Coughlin K, Marcus PS. 1996 Turbulent bursts in Couette-Taylor flow. *Physical Review Letters* **77**, 2214.
52. Meseguer A, Mellibovsky F, Avila M, Marques F. 2009 Instability mechanisms and transition scenarios of spiral turbulence in Taylor-Couette flow. *Physical Review E* **80**, 046315.
53. Avila K, Hof B. 2013 High-precision Taylor-Couette experiment to study subcritical transitions and the role of boundary conditions and size effects. *Review of Scientific Instruments* **84**, 065106.

54. Cross MC, Hohenberg PC. 1993 Pattern formation outside of equilibrium. *Reviews of Modern Physics* **65**, 851–1112.
55. Cross MC, Greenside H. 2009 *Pattern Formation and Dynamics in Nonequilibrium Systems*. Cambridge, UK: Cambridge University Press.
56. Mallock A. 1889 IV. Determination of the viscosity of water. *Proceedings of the Royal Society of London* **45**, 126–132.
57. Cole JA. 1976 Taylor-vortex instability and annulus-length effects. *Journal of Fluid Mechanics* **75**, 1–15.
58. Burin MJ, Ji H, Schartman E, Cutler R, Heitzenroeder P, Liu W, Morris L, Raftopolous S. 2006 Reduction of Ekman circulation within Taylor–Couette flow. *Experiments in Fluids* **40**, 962–966.
59. Benjamin TB. 1978 Bifurcation phenomena in steady flows of a viscous fluid. I. Theory, II. Experiments. *Proceedings of the Royal Society of London. A. Mathematical and Physical Sciences* **359**, 1–26, 27–43.
60. Benjamin TB, Mullin T. 1981 Anomalous modes in the Taylor experiment. *Proceedings of the Royal Society of London. A. Mathematical and Physical Sciences* **377**, 221–249.
61. Pfister G, Schmidt H, Cliffe KA, Mullin T. 1988 Bifurcation phenomena in Taylor–Couette flow in a very short annulus. *Journal of Fluid Mechanics* **191**, 1–18.
62. Mullin T, Toya Y, Tavener SJ. 2002 Symmetry-breaking and multiplicity of states in small aspect ratio Taylor–Couette flow. *Physics of Fluids* **14**, 2778–2787.
63. Pfister G, Buzug T, Enge N. 1992 Characterization of experimental time series from Taylor–Couette flow. *Physica D: Nonlinear Phenomena* **58**, 441–454.
64. Marques F, Lopez JM. 2006 Onset of three-dimensional unsteady states in small-aspect-ratio Taylor–Couette flow. *Journal of Fluid Mechanics* **561**, 255–277.
65. Abshagen J, Lopez JM, Marques F, Pfister G. 2005 Symmetry breaking via global bifurcations of modulated rotating waves in hydrodynamics. *Physical Review Letters* **94**, 074501.
66. Heise M, Abshagen J, Küter D, Hochstrate K, Pfister G, Hoffmann C. 2008 Localized spirals in Taylor–Couette flow. *Physical Review E* **77**, 026202.
67. Heise M, Hochstrate K, Abshagen J, Pfister G. 2009 Spirals vortices in Taylor–Couette flow with rotating endwalls. *Physical Review E* **80**, 045301.
68. Crowley CJ, Krygier MC, Borrero-Echeverry D, Grigoriev RO, Schatz MF. 2020 A novel subcritical transition to turbulence in Taylor–Couette flow with counter-rotating cylinders. *Journal of Fluid Mechanics* **892**.
69. Czarny O, Serre E, Bontoux P, Lueptow RM. 2002 Spiral and wavy vortex flows in short counter-rotating Taylor–Couette cells. *Theoretical and computational fluid dynamics* **16**, 5–15.
70. Kaneko K. 1985 Spatiotemporal intermittency in coupled map lattices. *Prog. Theor. Phys.* **74**, 1033–1044.
71. Bottin S, Daviaud F, Manneville P, Dauchot O. 1998 Discontinuous transition to spatiotemporal intermittency in plane Couette flow. *Europhysics Letters* **43**, 171.
72. Feynman RP, Leighton RB, Sands M. 1977 *The Feynman Lectures on Physics*, Vol. 2. Boston, MA: Addison-Wesley.
73. Burin MJ, Czarnocki CJ. 2012 Subcritical transition and spiral turbulence in circular Couette flow. *Journal of Fluid Mechanics* **79**, 106–122.
74. Prigent A, Grégoire G, Chaté H, Dauchot O, van Saarloos W. 2002 Large-scale finite-wavelength modulation within turbulent shear flows. *Phys. Rev. Lett.* **89**, 014501.
75. Tillmark N, Alfredsson PH. 1996 Experiments on rotating plane Couette flow. In Gavrilakis S, Machiels L, Monkewitz PA, editors, *Advances in Turbulence VI* Proceedings of the Sixth European Turbulence Conference p. 391–394. Kluwer Academic.
76. Litschke H, Roesner KG. 1998 New experimental methods for turbulent spots and turbulent spirals in the Taylor–Couette flow. *Experiments in fluids* **24**, 201–209.
77. Tsukahara T, Tillmark N, Alfredsson PH. 2010 Flow regimes in a plane Couette flow with system rotation. *Journal of Fluid Mechanics* **648**, 5–33.
78. Berghout P, Dingemans RJ, Zhu X, Verzicco R, Stevens RJAM, Van Saarloos W, Lohse D. 2020 Direct numerical simulations of spiral Taylor–Couette turbulence. *Journal of Fluid Mechanics* **887**.
79. Barkley D, Tuckerman LS. 2005 Computational study of turbulent-laminar patterns in Couette flow. *Physical Review Letters* **94**, 014502.
80. Avila M, Grimes M, Lopez JM, Marques F. 2008 Global endwall effects on centrifugally stable flows. *Physics of Fluids* **20**, 104104.

81. Avila M. 2012 Stability and Angular-Momentum Transport of Fluid Flows between Corotating Cylinders. *Physical Review Letters* **108**, 124501.
82. Lopez JM. 2016 Subcritical instability of finite circular Couette flow with stationary inner cylinder. *Journal of Fluid Mechanics* **793**, 589–611.
83. Schultz-Grunow F. 1959 Zur Stabilität der Couette-Strömung. *Zeitschrift für Angewandte Mathematik und Mechanik* **39**, 101–110.
84. Borrero-Echeverry D, Schatz MF, Tagg R. 2010 Transient turbulence in Taylor–Couette flow. *Physical Review E* **81**, 025301.
85. Peixinho J, Mullin T. 2006 Decay of Turbulence in Pipe Flow. *Physical Review Letters* **96**, 094501.
86. Hof B, Westerweel J, Schneider TM, Eckhardt B. 2006 Finite lifetime of turbulence in shear flows. *Nature (London)* **443**, 59–62.
87. Hof B, de Lozar A, Kuik DJ, Westerweel J. 2008 Repeller or attractor? Selecting the dynamical model for the onset of turbulence in pipe flow. *Physical Review Letters* **101**, 214501.
88. Avila M, Willis AP, Hof B. 2010 On the transient nature of localized pipe flow turbulence. *Journal of Fluid Mechanics* **646**, 127–136.
89. Alidai A, Greidanus AJ, Delfos R, Westerweel J. 2016 Turbulent Spot in Linearly Stable Taylor–Couette Flow. *Flow, Turbulence and Combustion* **96**, 609–619.
90. Goldenfeld N, Guttenberg N, Gioia G. 2010 Extreme fluctuations and the finite lifetime of the turbulent state. *Physical Review E: Statistical, Nonlinear, and Soft Matter Physics* **81**, 035304(R).
91. Gumbel EJ. 1958 *Statistics of Extremes*. New York, NY: Columbia University Press.
92. Nemoto T, Alexakis A. 2021 Do extreme events trigger turbulence decay? A numerical study of turbulence decay time in pipe flows. *Journal of Fluid Mechanics* **912**.
93. Gomé S, Tuckerman LS, Barkley D. 2022 Extreme events in transitional turbulence. *Philosophical Transactions of the Royal Society A* **380**, 20210036.
94. Moxey D, Barkley D. 2010 Distinct large-scale turbulent-laminar states in transitional pipe flow. *Proceedings of the National Academy of Sciences* **107**, 8091–8096.
95. Avila K, Moxey D, De Lozar A, Avila M, Barkley D, Hof B. 2011 The onset of turbulence in pipe flow. *Science* **333**, 192–196.
96. Shi L, Avila M, Hof B. 2013 Scale invariance at the onset of turbulence in Couette flow. *Physical Review Letters* **110**, 204502.
97. Lemoult G, Shi L, Avila K, Jalikop SV, Avila M, Hof B. 2016 Directed percolation phase transition to sustained turbulence in Couette flow. *Nature Physics* **12**, 254.
98. Avila K, Hof B. 2020 Second-Order Phase Transition in Counter-Rotating Taylor–Couette Flow Experiment. *Entropy* **23**, 58.
99. Tuckerman LS, Chantry M, Barkley D. 2020 Patterns in Wall-Bounded Shear Flows. *Annual Review of Fluid Mechanics* **52**, 343–367.
100. Nagata M. 1990 Three-dimensional finite-amplitude solutions in plane Couette flow: Bifurcation from infinity. *Journal of Fluid Mechanics* **217**, 519–527.
101. Faisst H, Eckhardt B. 2000 Transition from the Couette–Taylor system to the plane Couette system. *Physical Review E* **61**, 7227–7230.
102. Kreilos T, Eckhardt B. 2012 Periodic orbits near onset of chaos in plane Couette flow. *Chaos: An Interdisciplinary Journal of Nonlinear Science* **22**, 047505.
103. Clever RM, Busse FH. 1997 Tertiary and quaternary solutions for plane Couette flow. *Journal of Fluid Mechanics* **344**, 137–153.
104. Romanov VA. 1973 Stability of plane-parallel Couette flow. *Functional analysis and its applications* **7**, 137–146.
105. Lustro JRT, Kawahara G, van Veen L, Shimizu M, Kokubu H. 2019 The onset of transient turbulence in minimal plane Couette flow. *J. Fluid Mech.* **862**.
106. Kreilos T, Eckhardt B, Schneider TM. 2014 Increasing lifetimes and the growing saddles of shear flow turbulence. *Phys. Rev. Lett.* **112**, 044503.
107. Meseguer A, Mellibovsky F, Avila M, Marques F. 2009 Families of subcritical spirals in highly counter-rotating Taylor–Couette flow. *Physical Review E* **79**, 036309.
108. Deguchi K, Meseguer A, Mellibovsky F. 2014 Subcritical equilibria in Taylor–Couette flow. *Physical Review Letters* **112**, 184502.
109. Wang B, Ayats R, Deguchi K, Mellibovsky F, Meseguer A. 2022 Self-sustainment of coherent structures in counter-rotating Taylor–Couette flow. .
110. Reetz F, Kreilos T, Schneider TM. 2019 Invariant Solution underlying Oblique Stripe Patterns in Plane Couette Flow. *Nature Communications* **10**, 2277.

111. Kawahara G, Kida S. 2001 Periodic motion embedded in plane Couette turbulence: Regeneration cycle and burst. *Journal of Fluid Mechanics* **449**, 291–300.
112. Gibson JF, Halcrow J, Cvitanović P. 2008 Visualizing the geometry of state space in plane Couette flow. *Journal of Fluid Mechanics* **611**, 107–130.
113. Kawahara G, Uhlmann M, Van Veen L. 2012 The significance of simple invariant solutions in turbulent flows. *Annu. Rev. Fluid Mech.* **44**, 203–225.
114. Graham MD, Floryan D. 2021 Exact coherent states and the nonlinear dynamics of wall-bounded turbulent flows. *Annual Review of Fluid Mechanics* **53**, 227–253.
115. Krygier MC, Pughe-Sanford JL, Grigoriev RO. 2021 Exact coherent structures and shadowing in turbulent Taylor–Couette flow. *Journal of Fluid Mechanics* **923**, A7.
116. Crowley CJ, Pughe-Sanford JL, Toler W, Krygier MC, Grigoriev RO, Schatz MF. 2022a Turbulence tracks recurrent solutions. *Proceedings of the National Academy of Sciences* **119**, e2120665119.
117. Crowley CJ, Pughe-Sanford JL, Toler W, Grigoriev RO, Schatz MF. 2022b Observing a Dynamical Skeleton of Turbulence in Taylor–Couette Flow Experiments. (preprint, 10.48550/ARXIV.2208.10031).
118. Deguchi K. 2017 Linear instability in Rayleigh-stable Taylor–Couette flow. *Physical Review E* **95**, 021102.
119. Balbus SA. 2003 Enhanced Angular Momentum Transport in Accretion Disks. *Annual Review of Astronomy and Astrophysics* **41**, 555–597.
120. Ji H, Burin M, Schartman E, Goodman J. 2006 Hydrodynamic turbulence cannot transport angular momentum effectively in astrophysical disks. *Nature (London)* **444**, 343–346.
121. Paoletti MS, Lathrop DP. 2011 Angular momentum transport in turbulent flow between independently rotating cylinders. *Physical Review Letters* **106**, 024501.
122. Edlund EM, Ji H. 2014 Nonlinear stability of laboratory quasi-Keplerian flows. *Physical Review E* **89**, 021004.
123. Lopez JM, Avila M. 2017 Boundary-layer turbulence in experiments on quasi-Keplerian flows. *Journal of Fluid Mechanics* **817**, 21–34.
124. Canton J, Rinaldi E, Örlü R, Schlatter P. 2020 Critical point for bifurcation cascades and featureless turbulence. *Physical Review Letters* **124**, 014501.